

Packaging stiff polymers in small containers: A molecular dynamics study

D. C. Rapaport*

Department of Physics, Bar-Ilan University, Ramat-Gan 52900, Israel

(Dated: September 15, 2016)

The question of how stiff polymers are able to pack into small containers is particularly relevant to the study of DNA packaging in viruses. A reduced version of the problem based on coarse-grained representations of the main components of the system – the DNA polymer and the spherical viral capsid – has been studied by molecular dynamics simulation. The results, involving longer polymers than in earlier work, show that as polymers become more rigid there is an increasing tendency to self-organize as spools that wrap from the inside out, rather than the inverse direction seen previously. In the final state, a substantial part of the polymer is packed into one or more coaxial spools, concentrically layered with different orientations, a form of packaging achievable without twisting the polymer.

PACS numbers: 87.15.ap, 87.15.H-, 87.14.gk, 87.16.Ka

Consider a relatively stiff polymer chain being drawn into a small container through a narrow opening. This represents an idealized version of packing double-stranded (ds) DNA into the capsid of a large virus such as a bacteriophage [1–4]. Because the packing density is high and the virus must be able to eject the DNA at the end of its life cycle, ordered packaging of the polymer would appear advantageous. The basic physics question is, then, how do polymers pack in the absence of any imposed guiding mechanism? Experimental evidence suggests that DNA packaging involves organized large loops [5–8], and much has been learned from theory and modeling [9–17], but the chains simulated previously may not have been long enough to reveal what actually occurs.

MD (molecular dynamics) simulation is used here to investigate a simple packing model comprising a self-avoiding chain of linked spheres, subject to bond and bond-angle interactions, together with a spherical shell in which there is a small portal through which the chain enters, pulled inside by a suitable force. The goal is to determine whether ordered packing occurs spontaneously and if so, the dependence on the model parameters, principally the ratio of the chain dimensions (i.e., the persistence length) and the shell size. While this reduced problem omits many aspects of its real-world counterpart, including structural elements and complex short- and long-ranged interactions, details of which are not readily determined, any systematic behavior observed in the simulations could contribute to understanding the phenomenon.

Highly simplified models are essential for condensing entire packaging trajectories into timescales accessible to MD. A coarse-grained polymer model [18] is used that consists of a chain of $N = 8000$ spheres linked by elastic bonds of limited extensibility. The excluded-volume soft-sphere (SP) interaction is $U(r) = 4\epsilon[(\sigma/r)^{12} - (\sigma/r)^6] + \epsilon$ for sphere separation $r < r_c = 2^{1/6}\sigma$. Reduced MD units will be used subsequently: the sphere mass is unity, and

length, energy, time and temperature are expressed in terms of σ , ϵ , $\sigma/\sqrt{\epsilon}$ and ϵ/k_B . Adjacent chain spheres are bonded by a reversed pair of SP interactions with origins separated by 2.1; the measured mean bond length is $l_b = 1.051$ with a 3% variation. Chain bending is governed by the interaction $U(\theta) = 0.5f_a(\cos\theta - 1)^2$, where θ is the angle between adjacent bonds, with a minimum in the linear configuration ($\theta = 0$). The stiffness, f_a , is the only parameter varied in the present study; for $500 < f_a < 5000$ the measured persistence length, $L_p = l_b/(1 - \langle \cos\theta \rangle)$, ranges from 50 to 150. There is no torsional interaction to counter chain twist (important in real DNA), an omission that will be seen as fully justified by the results.

The capsid is represented as a fixed spherical shell with radius $R_s = 20$ which, for the stiffest chains, is much smaller than L_p ; a shell wall of thickness $\approx r_c$ is produced by a radial SP interaction originating at R_s . If $\sigma = 2.5\text{nm}$, a representative value for coarse-grained models of ds-DNA, then $R_s = 50\text{nm}$, a typical capsid size (the L_p range is then 125–375nm); chain segments forming a loop of this radius would have $\theta \approx 3^\circ$. Several (here 12) fixed spheres are embedded in the shell wall, in the equatorial plane (normal to the portal axis) and inset by r_c . Their task is to roughen the surface to oppose free rotation of the chain already packed into the shell during insertion (there is none after insertion ends); in the analogous macroscopic system [19] sliding friction prohibits rotation of this kind.

There is a small circular portal in the shell for chain entry. This hole is effectively a cylinder with unit radius and half-length, inside which a radial force pulls spheres into the shell, a simple approximation to nature's ATP-powered motor [1]; given its short length it can hold just two spheres. The force strength (here 1.4) is chosen to ensure slow, reasonably steady (and mainly unidirectional) transport through the portal and is the same for all runs. Portal geometry restricts the chain entry direction to below 45° from the normal; further reducing this angle using a longer cylinder would alter the outcome by directing the chain radially, a separate problem not con-

* rapaport@mail.biu.ac.il

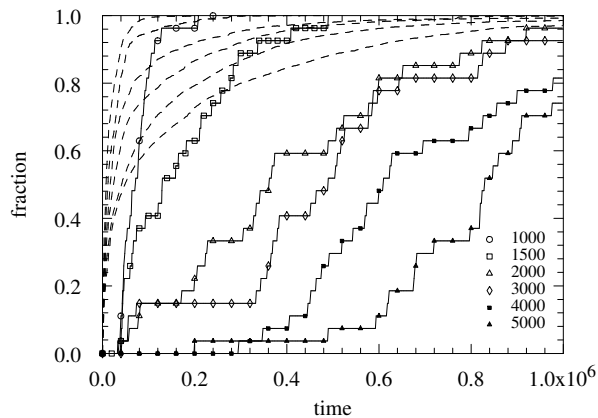


FIG. 1. Fraction of spheres inside shell (dashed lines, increasing f_a from left) and fraction of fully inserted chains vs time (reduced units).

sidered here. Similarly simplified models have been used in earlier work [12, 14, 16], although design details and computational methods differ.

Computations are carried out on a massively parallel GPU (graphics processing unit), where efficiency requires large systems, thus each simulation considers 27 independent chains simultaneously. The chains are confined to a box of size 360 with rigid walls; while far smaller than $l_b N$, the size is large enough ($> L_p$) that its effect on the strongly varying (prior to shell entry) chain conformation is minimal. The initial state of each chain is a closely spaced helix of radius $\approx R_s$ aligned with the portal, and the initial (≈ 40) spheres are redirected so the first few are inside the shell. Standard MD methods [18] are used, with a time step of 0.005 and a (constant- T) thermostat that maintains a temperature of $T = 0.4$; even when the stiffest chain is bent to fit inside the shell the mean bending energy remains well below the kinetic energy (0.6) despite L_p being several times R_s . Simulations are run for up to 2×10^8 steps, adequate for complete insertion of most chains. Snapshots of the coordinates are recorded periodically for analysis.

Figure 1 shows how the fractions of spheres inside the shell (averaged over all chains) and completely inserted chains depend on time, for several values of f_a covering a range from moderately flexible to sufficiently stiff chains that entry is seriously impeded. The mean insertion rate falls as chains become stiffer, a trend that persists to even higher f_a ; the typical insertion speed ≈ 0.01 is just 1% of $v_{\text{therm}} = \sqrt{3T}$, ensuring near-equilibrium conditions. Individual chain transport (not shown) can be extremely irregular, as observed experimentally [4]. The time required for complete insertion is also seen to be highly variable.

Radial density distributions, each averaged over all fully inserted chains and over 10 snapshots, are shown in Fig. 2. Depending on f_a , two or three peaks occur

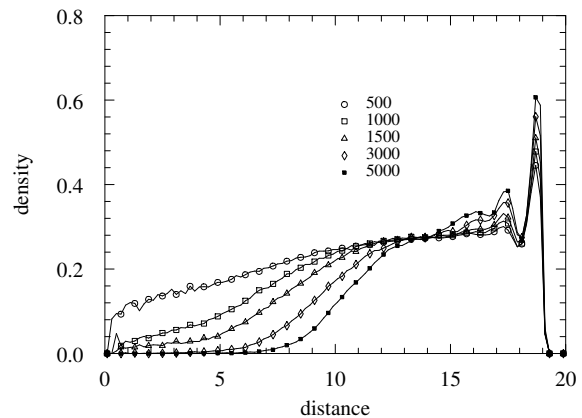


FIG. 2. Radial density distributions (reduced units) for several f_a values.

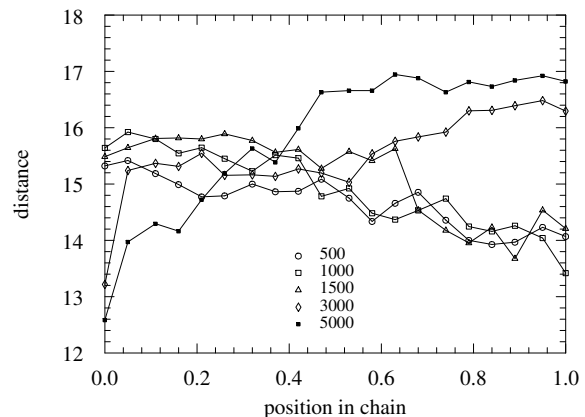


FIG. 3. Mean distance of chain spheres from the shell center as a function of (normalized) location along chain contour.

near multiples of r_c from the shell boundary, a signature of layering. Density drops towards the shell center, with an almost empty sphere of radius $\approx R_s/2$ for $f_a = 5000$, and increasingly broad distributions at lower f_a . Since the total chain volume, when approximated by a tube, is $N\pi r_c^2 \approx 6000$, ideally it would fill $\approx 20\%$ of the shell volume ($4\pi/3 R_s^3 \approx 32000$) when tightly packed, but Fig. 2 shows that even the stiffest chains actually expand to occupy 80% of the volume because the bending energy involved is small.

The question of where chain spheres are positioned is partially answered by Fig. 3 which shows their mean distance from the shell center as a function of location along the chain contour (averaged as before). The preferred packing direction changes with chain stiffness: for larger f_a chain segments that enter later lie on the outside (on average), while for smaller f_a the opposite is true, although the trend is weaker.

A more detailed explanation of how packaged chains

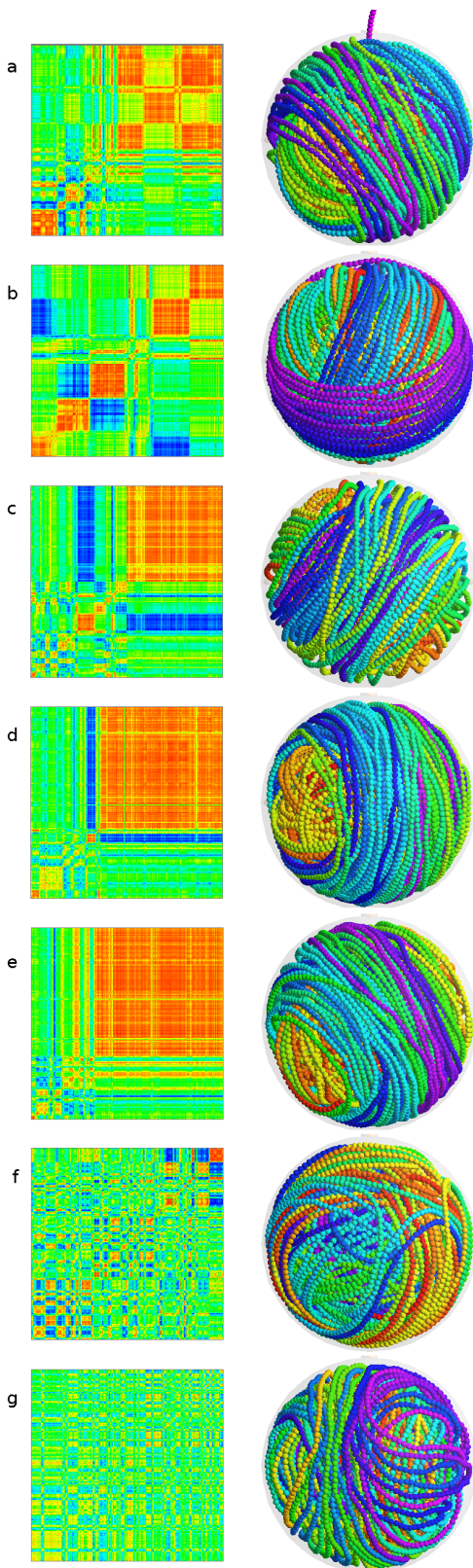


FIG. 4. Orientational correlation plots and pictures of selected chains; details and color schemes are explained in the text (in the grayscale print version, dark gray = blue/violet, medium gray = red, light gray = yellow/green); cases (a–e) are for $f_a = 5000$, (f,g) are for $f_a = 3000$ and 1000 .

are organized appears in Fig. 4, where pictures of chain configurations are paired with orientational correlation plots (explained below). The shell envelope is shown semi-transparently with the portal at the top. Spectral colors are used for the chain configurations, ranging from red at the chain head (the segments that enter first) to violet at the tail; thus the image of a chain whose tail is adjacent to the shell wall typically has red segments inside and violet loops on the outside, with the other colors interspersed. Note that static pictures cannot reveal slow time-dependent behavior such as rotation of the partially packaged chain, or spool rearrangement during and after insertion that can obscure the final stages of the insertion history; animated image sequences provide additional information.

Long chain sections arranged into spool-like configurations are a prominent feature of the imagery, a mode of organization that can be quantified using orientational correlation functions. These are evaluated by considering successive chain segments i of length (e.g.) 40 ($1 \leq i \leq 200$) and, on the assumption that each segment is approximately planar, evaluating its normal \vec{n}_i as the mean of the cross products of vectors between spheres in the segment spaced (e.g.) four apart. A (symmetric) matrix \mathbf{C} is constructed, where $C_{ij} = \arccos(\vec{n}_i \cdot \vec{n}_j)$ is the angle between the normals of segments i and j , and displayed as a 2D plot with color denoting angular ranges (these colors unrelated to the pictures); the chain head is in the lower-left corner. The i th row/column shows the alignment of chain segments relative to i , where three segments amount to a single loop around the shell. Regions of the chain with near-parallel alignment, the usual case for contiguous segments that tend to be strongly correlated (except when an abrupt change occurs), are shown in red, regions oriented antiparallel (to the original) in blue, and intermediate cases in yellow and green.

The color plots do not show where individual segments are located in the shell, but by comparing each \mathbf{C} with its picture it is apparent that a large upper-right red square corresponds to a section of the chain forming a spool with multiple loops in contact with, or close to, the shell wall; this, in turn, may be wrapped around one or more differently aligned interior spools, typically terminating in a region with minimal correlation extending to the chain head. Brief interruptions in the large red squares correspond to short misaligned sections, sometimes just a single loop. The variety of organizational patterns is unsurprising since the packed state represents the outcome of a sequence of individual events that have little or no temporal relation; a typical event might be a choice between a chain segment forcing previously packed contents to rotate so that it can be accommodated on the exterior with minimal bending, or the opening of a gap between loops so that it can penetrate to the interior.

Examples (a–e) are for the stiffest chains considered ($f_a = 5000$, the results for $f_a = 4000$ are similar). Case (a) shows a chain just prior to complete insertion with the final tail segment traversing the portal. Cases (b–e)

show fully inserted chains with increasingly large ordered regions. Each chain is packed differently; 22 of the 27 chains exceed 99% completion (for this f_a), and in 12 of them the upper-right square of \mathbf{C} is a red or red/yellow block that includes at least half the chain, apart from a few defects, indicating that the dominant feature is a single spool. In case (b) there are several smaller blocks corresponding to shorter spools, concentrically arranged with differing orientations. In general, sets of spooled loops with (near-) maximal radius form in (or close to) a median plane passing through the portal; the spool axis direction varies slightly but can persist for a relatively long time before undergoing sudden change. Previously inserted chain segments form a soft, fluctuating ‘core’ that rotates slowly and unevenly to accommodate new segments, usually on or close to the outside. Note that twisting of the chain is not required, justifying the omission of any torsional interaction; the minimal influence of torsion is described in [20]. The measured increasing mean radial distance as a function of sphere location in the chain (Fig. 3) is consistent with these observations.

The initial section of the chain to enter (up to ≈ 4000 spheres, typically exceeding the longest chains considered in previous work) also forms loops, although the ordering is much weaker, and the loops are anisotropically compressed by subsequent chain segments. This could indicate the existence of an interior ‘framework’ that assists spooling, implying a minimal chain length for spool development. The behavior is the opposite of ‘inverse spooling’ – packing from the outside in – seen in simulations of shorter chains [12, 16, 17], even though

concentric spools form in both cases. The presence of multiple sets of spooled loops with various orientations allows more uniform coverage of the shell surface and reduces the bending energy (for both normal and inverse spools). The number of loops, assuming they span the full circumference, is $l_b N / 2\pi R_s \approx 70$.

The final two examples (f,g) are for more flexible chains, with $f_a = 3000$ and 1000 . Packaging is less ordered at lower f_a , and loops with higher curvature appear more often, so that while there is still some alignment, sizable spools are less likely. The spheres also have reduced energetic preference as to initial placement after insertion, so that the likelihood of the tail end of the chain being near the wall is lower (Fig. 3).

In conclusion, the fact that the complex mechanisms employed by viruses for packaging their genetic payloads are not readily understood has led to the development of reduced models aimed at capturing the principal features. Simulations of such a model reveal that spool-like organization appears spontaneously when packaging stiff polymer chains, with the late-entering part of the chain preferably located close to the shell wall. The efficacy of this packing scheme is obvious, in particular because the core rotation alleviates the need to overcome chain twisting, although it has not been considered previously. Apart from possible biological relevance, the results provide another example [21] of emergent cooperativity in the simplest of physical systems.

This work was initiated at the Aspen Center for Physics Workshop on Viral Assembly; the hospitality of the Center and partial support from NSF grant PHYS-1066293 is acknowledged.

-
- [1] C. M. Knobler and W. M. Gelbart, *Annu. Rev. Phys. Chem.* **60**, 367 (2009).
- [2] D. Marenduzzo, C. Micheletti, and E. Orlandini, *J. Phys.: Condens. Matter* **22**, 283102 (2010).
- [3] J. A. Speir and J. E. Johnson, *Cur. Opin. Struct. Biol.* **22**, 65 (2012).
- [4] Z. T. Berendsen, N. Keller, S. Grimes, P. J. Jardine, and D. E. Smith, *PNAS* **111**, 8345 (2014).
- [5] K. E. Richards, R. C. Williams, and R. Calendar, *J. Mol. Biol.* **78**, 255 (1973).
- [6] W. C. Earnshaw and S. C. Harrison, *Nature* **268**, 598 (1977).
- [7] M. E. Cerritelli, N. Cheng, A. H. Rosenberg, C. E. McPherson, F. P. Booy, and A. C. Steven, *Cell* **91**, 271 (1997).
- [8] G. C. Lander, L. Tang, S. R. Casjens, E. B. Gilcrease, P. Prevelige, A. Poliakov, C. S. Potter, B. Carragher, and J. E. Johnson, *Science* **312**, 1791 (2006).
- [9] P. K. Purohit, J. Kondev, and R. Phillips, *PNAS* **100**, 3173 (2003).
- [10] A. Ben-Shaul, *Biophys. J.* **104**, L15 (2013).
- [11] J. Kindt, S. Tzlil, A. Ben-Shaul, and W. M. Gelbart, *PNAS* **98**, 13671 (2001).
- [12] A. J. Spakowitz and Z.-G. Wang, *Biophys. J.* **88**, 3912 (2005).
- [13] I. Ali, D. Marenduzzo, and J. M. Yeomans, *Phys. Rev. Lett.* **96**, 208102 (2006).
- [14] C. Forrey and M. Muthukumar, *Biophys. J.* **91**, 25 (2006).
- [15] C. R. Locker and S. C. Harvey, *Multiscale Model. Simul.* **5**, 1264 (2006).
- [16] A. S. Petrov, M. B. Boz, and S. C. Harvey, *J. Struct. Biol.* **160**, 241 (2007).
- [17] J. P. Mahalik, B. Hildebrandt, and M. Muthukumar, *J. Biol. Phys.* **39**, 229 (2013).
- [18] D. C. Rapaport, *The Art of Molecular Dynamics Simulation*, 2nd ed. (Cambridge University Press, Cambridge, 2004).
- [19] N. Stoop, J. Najafi, F. K. Wittel, M. Habibi, and H. J. Herrmann, *Phys. Rev. Lett.* **106**, 214102 (2011).
- [20] G. C. Rollins, A. S. Petrov, and S. C. Harvey, *Biophys. J.* **94**, L38 (2008).
- [21] D. C. Rapaport, *J. Phys.: Condens. Matter* **26**, 503104 (2014).